Available online at www.sciencedirect.com
ScienceDirect
Electrochimica Acta 52 (2007) 6700–6706
ELECTROCHIMICA Acta
www.elsevier.com/locate/electacta

The improved electrochemical properties of novel La–Mg–Ni-based hydrogen storage composites

Hai-Liang Chu [a,b], Shu-Jun Qiu [a,b], Li-Xian Sun [a,c,*], Yao Zhang [a,*], Fen Xu [a], Tao Jiang [a,b], Wei-Xue Li [d], Min Zhu [e], Wang-Yu Hu [f]

[a] *Materials and Thermochemistry Laboratory, Dalian Institute of Chemical Physics, Chinese Academy of Sciences, Dalian 116023, China*
[b] *Graduate School of Chinese Academy of Sciences, Beijing 100049, China*
[c] *Department of Chemistry, Institute of Nanochemistry, Jinan University, Guangzhou 510632, China*
[d] *State Key Laboratory of Catalysis and Center for Theoretical and Computational Chemistry, Dalian Institute of Chemical Physics, Chinese Academy of Sciences, Dalian 116023, China*
[e] *School of Mechanical Engineering, South China University of Technology, Guangzhou 510641, China*
[f] *Department of Applied Physics, Hunan University, Changsha 410082, China*

Received 9 February 2007; received in revised form 20 April 2007; accepted 21 April 2007
Available online 3 May 2007

Abstract

In the present study, a novel alloy composite has been synthesized by ball milling nonstoichiometric AB_3-type $La_{0.7}Mg_{0.3}Ni_{3.5}$ alloy with $Ti_{0.17}Zr_{0.08}V_{0.35}Cr_{0.1}Ni_{0.3}$ alloy in order to improve the cyclic stability and other electrochemical properties of $La_{0.7}Mg_{0.3}Ni_{3.5}$ alloy electrode. The phase structure, morphology and electrochemical performances of the composite have been investigated systematically. From X-ray diffraction (XRD) patterns, it can be found that the $La_{0.7}Mg_{0.3}Ni_{3.5}$ and $Ti_{0.17}Zr_{0.08}V_{0.35}Cr_{0.1}Ni_{0.3}$ alloys still retain their respective phase structures in the composite. Electrochemical studies show that the cyclic stability of the composite electrode is noticeably improved after 100 charge–discharge cycles in comparison with single $La_{0.7}Mg_{0.3}Ni_{3.5}$ alloy electrode due to enhanced anti-corrosion performance in the alkaline electrolyte. The discharge capacity retention rate C_{100}/C_{max} of composite electrode is 62.3%, which is much higher than that of the $La_{0.7}Mg_{0.3}Ni_{3.5}$ alloy electrode, although the maximum discharge capacity of the former decreases moderately. Both electrochemical impedance spectra (EIS) and linear polarization (LP) studies indicate that the electrochemical kinetics of the composite electrode is also improved. The charge-transfer resistance (R_{ct}), the polarization resistance (R_p) and the exchange current density (I_0) of the composite electrode are 160.2 mΩ, 129.5 mΩ and 201.6 mA/g, respectively, which are superior to those of the $La_{0.7}Mg_{0.3}Ni_{3.5}$ alloy electrode.

Keywords: Ni/MH batteries; La–Mg–Ni hydrogen storage alloy; Composite; Electrochemical properties; Electrochemical kinetics; Corrosion behaviors

1. Introduction

In recent years, the AB_3-type La–Mg–Ni-based hydrogen storage alloys were extensively studied as negative electrode candidates for Ni–MH secondary batteries due to their higher discharge capacities [1–8]. For example, the investigations on nonstoichiometric La–Mg–$(NiCo)_x$ ($x = 3$–3.5) series alloys by Kohno et al. [1] indicated that the maximum electrochemical discharge capacity of the $La_{0.7}Mg_{0.3}Ni_{2.8}Co_{0.5}$ alloy reached 410 mAh/g, which was much higher than that of conventional AB_5-type hydrogen storage alloys. Chen et al. [5] investigated the structural and electrochemical characteristics of the $LaCaMg(NiM)_9$ (M = Al, Mn) alloys which reached a maximum discharge capacity of 356 mAh/g. However, these La–Mg–Ni-based hydrogen storage alloy electrodes suffer from serious degradation of discharge capacity during the charge–discharge cycles. In order to improve the cyclic stability of La–Mg–Ni-type hydrogen storage alloy electrodes, the partial substitution of nickel with many transition metals such as cobalt, manganese, iron, copper, aluminum, zinc, etc. [9–11] and the partial substitution of lanthanum with cerium [12,13] or zirconium [14] have been carried out extensively. However,

* Corresponding authors at: Materials and Thermochemistry Laboratory, Dalian Institute of Chemical Physics, Chinese Academy of Sciences, Dalian 116023, China. Tel.: +86 411 84379213/84379215; fax: +86 411 84379213.
E-mail addresses: lxsun@dicp.ac.cn (L.-X. Sun), zhangyao@dicp.ac.cn (Y. Zhang).

0013-4686/$ – see front matter © 2007 Elsevier Ltd. All rights reserved.
doi:10.1016/j.electacta.2007.04.097

the cyclic stability of the alloy electrodes is still unsatisfactory.

Meanwhile, the Ti–V-based multiphase hydrogen storage alloys were paid much attention, which generally consist of a C14 Laves phase and a V-based solid solution phase. The V-based solid solution phase is the major hydrogen-absorbing phase, while the C14 Laves phase is not only a hydrogen-absorbing phase, but also works as a catalyst for the electrochemical hydrogenation and dehydrogenation process of the V-based phase [15–17]. The synergistic effect of the two phases gives the alloy a favorable electrochemical performance, especially the discharge capacity. Moreover, the Ti–V-based alloy electrodes have improved cyclic stability during the charge–discharge cycles. For example, the discharge capacity retention after 50 cycles of $Ti_{0.17}Zr_{0.08}V_{0.35}Cr_{0.1}Ni_{0.3}$ alloy electrode is 97% and 95% at 303 K and 313 K, respectively [18]. Therefore, it can be expected that the overall electrochemical properties, especially the cyclic stability, of the La–Mg–Ni-type hydrogen storage alloys could be improved through the formation of composite with Ti–V-based multiphase hydrogen storage alloy.

In this paper, the $La_{0.7}Mg_{0.3}Ni_{3.5}$ and $Ti_{0.17}Zr_{0.08}V_{0.35}Cr_{0.1}Ni_{0.3}$ alloys were served as parent alloys and the composite was successfully prepared by ball milling the mixture of both alloys powder. The structure, corrosion behaviors and the electrochemical properties of the as-prepared composite were investigated systematically.

2. Experimental

Hydrogen storage alloys of nominal composition $La_{0.7}Mg_{0.3}Ni_{3.5}$ and $Ti_{0.17}Zr_{0.08}V_{0.35}Cr_{0.1}Ni_{0.3}$ were prepared by vacuum magnetic levitation melting under high purity argon atmosphere from component metals with the purity all above 99.5%. To assure the homogeneity of these two alloys, the ingots were turned over and remelted three times. The ingot was thus mechanically crushed in air and ground into the powder of 200-mesh size. The composite was prepared by ball milling the homogenous mixture of $La_{0.7}Mg_{0.3}Ni_{3.5}$ and $Ti_{0.17}Zr_{0.08}V_{0.35}Cr_{0.1}Ni_{0.3}$ in the weight ratio of 1:1, which was performed upon QM-1SP planetary ball miller under 0.2–0.3 MPa argon atmosphere for 10 min. In each stainless milling pot, the ball-to-powder weight ratio was 20:1. The crystal structure of the parent alloys and as-prepared composite was characterized by XRD (Rigaku D/max-2500, Cu Kα, 40 kV, 250 mA). The surface morphology of the composite was observed using scanning electron microscopy (SEM, JSM6360LV) linked with energy dispersive X-ray spectrometer (EDS, Oxford INCA).

The tested electrodes for electrochemical measurements were fabricated by mixing 100 mg alloy powder with 300 mg electrolytic Ni powder. The mixture was then pressed into a circular pellet of 10 mm in diameter under a pressure of 30 MPa. The electrode pellet was then pressed with two foam nickel sheets at a pressure of 6 MPa and tightly spot-welded. A nickel lead wire was attached to this pressed foam nickel sheet by spot welding. Electrochemical measurements were performed in a standard open tri-electrode electrolysis cell consisting of a working electrode (the MH pellet electrode for studying), a sintered $Ni(OH)_2$/NiOOH counter electrode, and a Hg/HgO reference electrode. The temperature was controlled at 303 K (±0.5 K) and the electrolyte was 6 M KOH solution. Charge–discharge cycles of alloy electrodes were conducted by an automatic LAND battery test instrument (CT2001A). The electrodes were charged for 3 h at a current density of 300 mA/g, rested for 5 min and then discharged to the cut-off potential of −0.6 V (versus Hg/HgO reference electrode) at a current density of 100 mA/g.

The open circuit potentials of the electrodes were recorded immediately after immersing the electrode into the KOH solution until the potentials of the electrodes tend to be constant. The anodic polarization curves were measured at 0.1 mV/s from 0 mV to 20 mV (versus open circuit potential) after the electrodes were immersed in KOH solution for 10 h in order to obtain the corrosion current of the electrode. The linear polarization (LP) curves of the alloy electrodes were measured on a Zahner Elektrik IM6e electrochemical workstation by scanning the electrode potential at a rate of 0.1 mV/s from −5 mV to 5 mV (versus open circuit potential) at 50% depth of discharge (DOD). To investigate the alloy electrode kinetics, the electrochemical impedance spectroscopy (EIS) studies were conducted from 10 kHz to 5 mHz with an amplitude of 5 mV versus open circuit potential at 50% DOD using the IM6e electrochemical workstation. Before EIS measurements, the electrodes were first fully activated by charge/discharge for five cycles.

3. Results and discussion

3.1. The phase structure and morphology of the composite

Fig. 1 shows that X-ray diffraction patterns of the $La_{0.7}Mg_{0.3}Ni_{3.5}$ alloy, $Ti_{0.17}Zr_{0.08}V_{0.35}Cr_{0.1}Ni_{0.3}$ alloy, and the as-prepared composite. From Fig. 1(a), it is found that the $La_{0.7}Mg_{0.3}Ni_{3.5}$ alloy mainly consists of the $(LaMg)Ni_3$ phase with the $PuNi_3$-type rhombohedral structure (space group *R*-3*m*), the $LaNi_5$ phase with the $CaCu_5$-type hexagonal structure (space group *P*6/*mmm*) and the LaNi phase with the orthorhombic CrB-type structure (space group *Cmcm*). This result is consistent with that reported by Pan et al. [19]. It is also found that the $Ti_{0.17}Zr_{0.08}V_{0.35}Cr_{0.1}Ni_{0.3}$ alloy is mainly composed of V-based solid solution with BCC phase (space group *Im*3*m*) and C14 Laves phase with $MgZn_2$-type structure (space group $P6_3/mmc$). After ball milling the powder mixture of $La_{0.7}Mg_{0.3}Ni_{3.5}$ and $Ti_{0.17}Zr_{0.08}V_{0.35}Cr_{0.1}Ni_{0.3}$ (weight ratio 1:1) for 10 min, both $La_{0.7}Mg_{0.3}Ni_{3.5}$ and $Ti_{0.17}Zr_{0.08}V_{0.35}Cr_{0.1}Ni_{0.3}$ basically maintain their respective original phase structures in the composite. No new phase forms in the composite after ball milling treatment according to the XRD detection.

Fig. 2 shows the SEM images and the corresponding EDS pattern of the composite. It is found that the composite particles are pulverized to the size of less than 50 μm. The EDS pattern of the micro-region in (b) is shown in (c). All elements in the composite are detected in the EDS pattern and their abundances agree with those of as-designed composite very well (see Table 1).

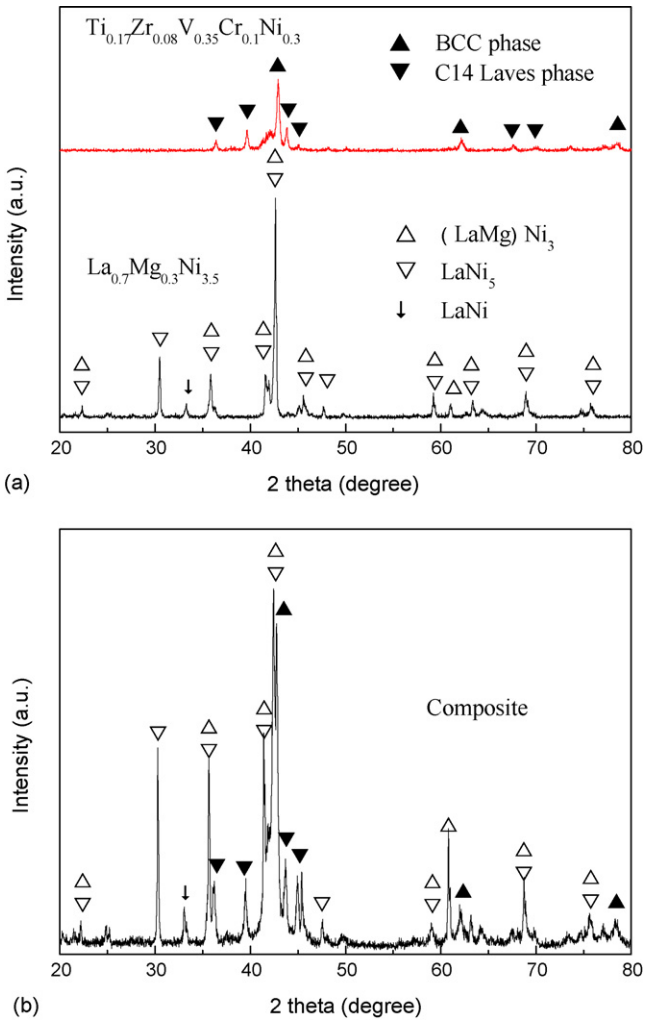

Fig. 1. XRD patterns of the $La_{0.7}Mg_{0.3}Ni_{3.5}$ alloy, $Ti_{0.17}Zr_{0.08}V_{0.35}Cr_{0.1}Ni_{0.3}$ alloy, and the composite.

3.2. Discharge capacity and cyclic stability

Fig. 3 presents the discharge potential curves of $La_{0.7}Mg_{0.3}Ni_{3.5}$ alloy, $Ti_{0.17}Zr_{0.08}V_{0.35}Cr_{0.1}Ni_{0.3}$ alloy, and the composite electrodes at the largest discharge capacity at 303 K. The maximum discharge capacities are 362.7 mAh/g and 335.7 mAh/g for $La_{0.7}Mg_{0.3}Ni_{3.5}$ alloy electrode and $Ti_{0.17}Zr_{0.08}V_{0.35}Cr_{0.1}Ni_{0.3}$ alloy electrode, respectively. Moreover, they have different discharge potentials, i.e., −0.8969 V for $La_{0.7}Mg_{0.3}Ni_{3.5}$ alloy electrode and −0.8725 V for $Ti_{0.17}Zr_{0.08}V_{0.35}Cr_{0.1}Ni_{0.3}$ alloy electrode at 50% depth of discharge (DOD). The composite electrode in this work has a maximum discharge capacity of 319.9 mAh/g and a discharge potential of −0.8969 V at 50% DOD. The discharge potential of the composite electrode is the same as that of the $La_{0.7}Mg_{0.3}Ni_{3.5}$ alloy electrode and lower than that of $Ti_{0.17}Zr_{0.08}V_{0.35}Cr_{0.1}Ni_{0.3}$ alloy electrode ($\Delta E_{50\%DOD} = 0.0247$ V). This phenomenon indicates that the composite is not the simple mixture of $La_{0.7}Mg_{0.3}Ni_{3.5}$ and $Ti_{0.17}Zr_{0.08}V_{0.35}Cr_{0.1}Ni_{0.3}$ alloys.

Table 1
The element abundance of the composite

	Elements						
	La	Mg	Ni	Ti	Zr	V	Cr
Calculated (wt.%)[a]	16.34	0.89	48.59	7.71	5.90	16.39	4.20
Experimental (wt.%)[b]	15.68	1.17	48.84	7.26	6.50	15.89	4.64

[a] The values calculated from the $La_{0.7}Mg_{0.3}Ni_{3.5}$ and $Ti_{0.17}Zr_{0.08}V_{0.35}Cr_{0.1}Ni_{0.3}$ alloys in the weight ratio of 1:1.
[b] The values from the EDS patterns.

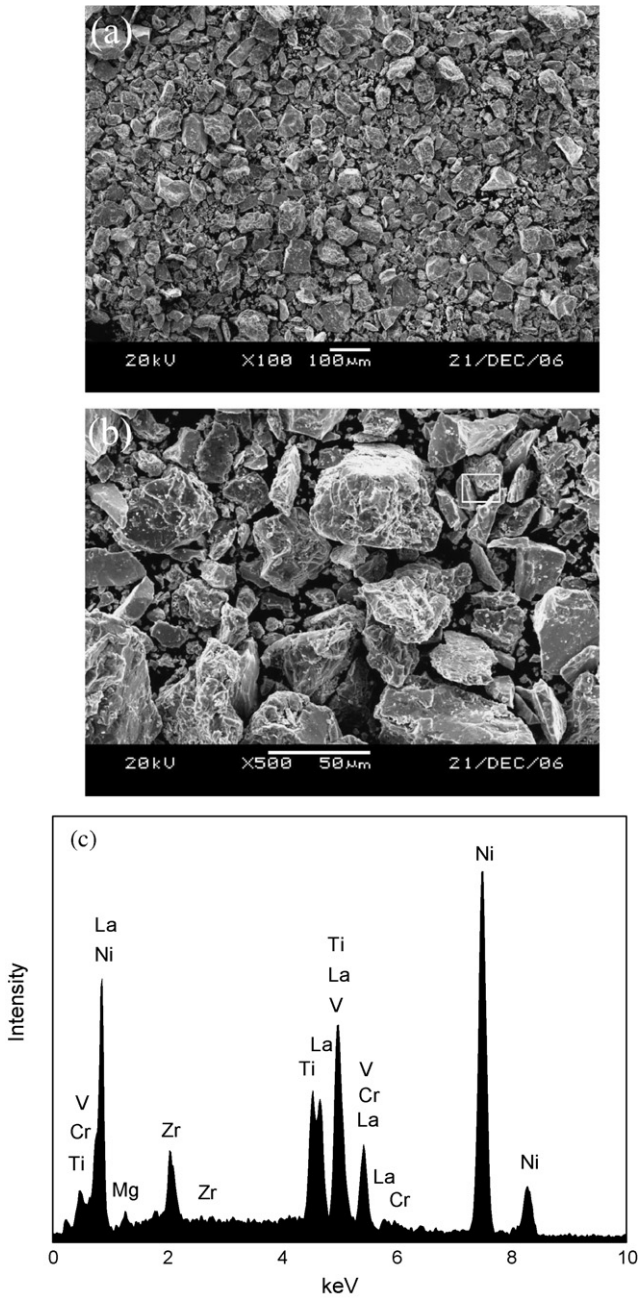

Fig. 2. SEM micrographs and EDS pattern of the composite.

Fig. 4 exhibits cyclic stability curves of $La_{0.7}Mg_{0.3}Ni_{3.5}$ alloy, and the composite electrodes at 303 K. The electrochemical characteristics of these two electrodes are summarized in

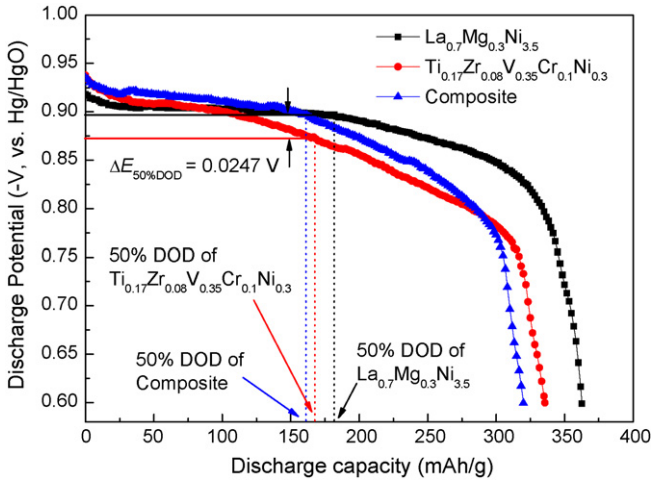

Fig. 3. Discharge potential curves of $La_{0.7}Mg_{0.3}Ni_{3.5}$, $Ti_{0.17}Zr_{0.08}V_{0.35}Cr_{0.1}Ni_{0.3}$, and the composite electrodes at the largest discharge capacity at 303 K.

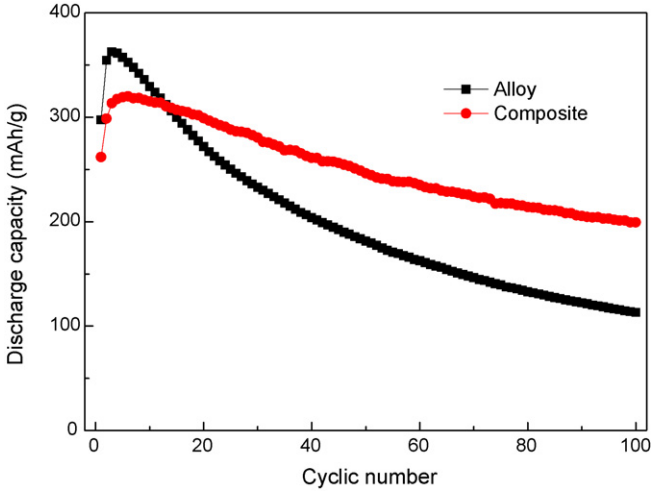

Fig. 4. The cyclic stability curves of $La_{0.7}Mg_{0.3}Ni_{3.5}$ alloy and the composite electrodes at 303 K.

Table 2. These electrodes can be fully activated within five charge–discharge cycles. It is found that the cyclic stability of the composite electrode is greatly enhanced compared with that of $La_{0.7}Mg_{0.3}Ni_{3.5}$ alloy, though its maximum discharge capacity is lower than that of $La_{0.7}Mg_{0.3}Ni_{3.5}$ alloy. For example, after 100 charge–discharge cycles, the discharge capacity retention rate of composite electrode increases significantly to 62.3%, which is much higher than that of the $La_{0.7}Mg_{0.3}Ni_{3.5}$ alloy electrode of 31.2%. It indicates that the $Ti_{0.17}Zr_{0.08}V_{0.35}Cr_{0.1}Ni_{0.3}$ alloy in the composite plays an important role in improving cyclic stability of the composite electrode.

Table 2
The electrochemical properties of the $La_{0.7}Mg_{0.3}Ni_{3.5}$ alloy and composite electrodes at 303 K

Samples	C_{max} (mAh/g)	N_a[a]	C_{50}/C_{max} (%)	C_{100}/C_{max} (%)
Alloy	362.7	3	50.0	31.2
Composite	319.9	5	77.0	62.3

[a] The cycle numbers needed to activate the electrodes.

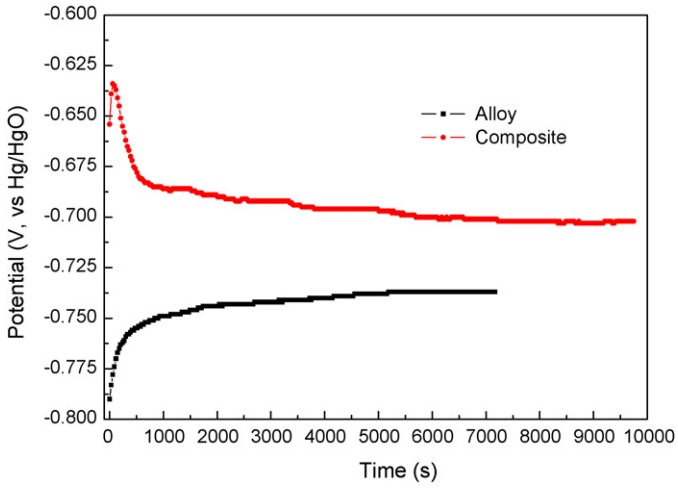

Fig. 5. The open circuit potentials of the $La_{0.7}Mg_{0.3}Ni_{3.5}$ alloy and composite electrodes at 303 K after immediately immersing in 6 M KOH solution.

3.3. Corrosion behaviors of as-prepared composite electrode

The corrosion potentials of the electrodes were determined by open circuit potential measurements, which started immediately after the alloy electrodes immersed in KOH solution [20,21]. Fig. 5 is the plot of the open circuit potentials V as a function of time t for the electrodes. It can be seen that the open circuit potentials are stabilized after about 2 h. However, the curves of the open circuit potential versus time are totally different from each other, which indicate again that the composite is not the simple mixture of $La_{0.7}Mg_{0.3}Ni_{3.5}$ and $Ti_{0.17}Zr_{0.08}V_{0.35}Cr_{0.1}Ni_{0.3}$ alloys. The open circuit potential (i.e., the corrosion potential) is −0.737 V for the $La_{0.7}Mg_{0.3}Ni_{3.5}$ alloy electrode. It is obvious that corrosion potential of the composite electrode is −0.702 V, which shifts towards more positive direction compared to the former. It is generally accepted that more positive corrosion potential results in the improved anti-corrosion performance of the electrode [20–22]. Therefore, the composite electrode has an enhanced anti-corrosion behavior than that of the $La_{0.7}Mg_{0.3}Ni_{3.5}$ alloy electrode, which enhances the cyclic stability of the composite electrode.

The corrosion currents of $La_{0.7}Mg_{0.3}Ni_{3.5}$ alloy and the composite electrodes were investigated by anodic polarization measured after the electrodes were immersed in the 6 M KOH solution for 10 h. The obtained curves are nonlinear fitted with Bulter–Volmer equation (Eq. (1)) using Levenberg–Marquardt algorithm. The corrosion current I_{corr} and the Tafel constant b_a, b_c are the fitted parameters in the Bulter–Volmer equation [23]:

$$I = I_{corr}\left[\exp\left(\frac{2.303\Delta E}{b_a}\right) - \exp\left(\frac{-2.303\Delta E}{b_c}\right)\right] \quad (1)$$

where I, ΔE are experimentally obtained current and overpotential, respectively.

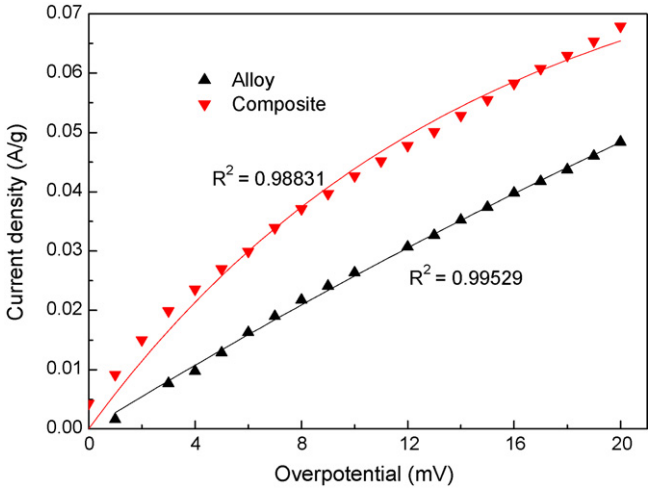

Fig. 6. The anode polarization curves (the dots) and the fitting results (the lines) of the $La_{0.7}Mg_{0.3}Ni_{3.5}$ alloy and composite electrodes at 303 K after immersing in KOH solution for 10 h.

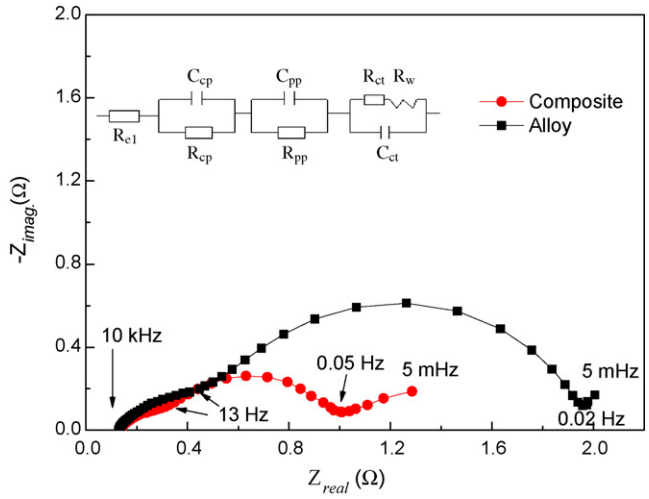

Fig. 7. The electrochemical impedance spectra (EIS) of the $La_{0.7}Mg_{0.3}Ni_{3.5}$ alloy and composite electrodes at 50% DOD and 303 K.

Fig. 6 exhibits the anodic polarization curves and their fitting results of the $La_{0.7}Mg_{0.3}Ni_{3.5}$ alloy and the composite electrodes at 303 K after immersing in KOH solution for 10 h. It can be seen that the fitting results match the experimental data very well. The corrosion current I_{corr} of the composite electrode is 0.0862 A/g, which is much lower than that of the $La_{0.7}Mg_{0.3}Ni_{3.5}$ alloy electrode (0.207 A/g). This indicates once again that the composite electrode has an improved anti-corrosion performance, which is consistent with the result of the corrosion potential measurement.

From the measurements of corrosion potential and corrosion current described above, it can be concluded that the formation of composite after ball milling the $La_{0.7}Mg_{0.3}Ni_{3.5}$ with $Ti_{0.17}Zr_{0.08}V_{0.35}Cr_{0.1}Ni_{0.3}$ alloy enhances the anti-corrosion behaviors of the electrodes, which further leads to the improvement of the cyclic stability of the composite electrode in Fig. 3.

3.4. The kinetics of the electrochemical reaction

Fig. 7 illustrates the electrochemical impedance spectra of the $La_{0.7}Mg_{0.3}Ni_{3.5}$ alloy and composite electrodes at 50% DOD and 303 K. Both the EIS spectra of these two electrodes consist of a smaller semicircle in the high-frequency region and a larger semicircle in the low-frequency region followed by a straight line. The EIS data were analyzed using an equivalent circuit as that proposed by Kuriyama et al. [24] and used by Tian et al. [25] (see the inset in Fig. 7). The capacitive components labeled by C are modeled as constant-phase elements (CPE) to describe the depressed nature of the semicircles. R_{el} is ascribed to the electrolyte resistance between the MH electrode and the reference electrode. The semicircle in the high-frequency region, modeled by R_{cp} and C_{cp}, results from the contact resistance between the alloy particles and the current collector. The contact resistance and capacitance between the alloy particles generate the parameters R_{pp} and C_{pp}, respectively. R_{ct} and C_{ct}, representing the semicircle in the low-frequency region, contribute to the charge-transfer reaction resistance and the double-layer capacitance, respectively. R_w is the Warburg impedance.

The parameters in the equivalent circuit were calculated by a nonlinear least squares fit using the simulation software of IM6e workstation. The contact resistance R_{pp} between alloy particles and charge-transfer reaction resistance R_{ct} of the electrodes are summarized in Table 3. The R_{pp} and R_{ct} are 747.1 mΩ and 327.8 mΩ for the $La_{0.7}Mg_{0.3}Ni_{3.5}$ alloy electrode, respectively. However, when the $Ti_{0.17}Zr_{0.08}V_{0.35}Cr_{0.1}Ni_{0.3}$ alloy is ball milled with $La_{0.7}Mg_{0.3}Ni_{3.5}$ alloy for 10 min, the electrochemical reaction kinetics of the composite electrode is improved, which behaves in two respects according to EIS. On the one hand, the introduction of the $Ti_{0.17}Zr_{0.08}V_{0.35}Cr_{0.1}Ni_{0.3}$ alloy into the composite decreases the contact resistance R_{pp} between alloy particles to 334.2 mΩ. On the other hand, the charge-transfer reaction resistance R_{ct} of the composite electrode is decreased to 160.2 mΩ, which indicates that the reaction rate on the surface of the alloy electrode increases resulting from formation of the composite after the addition of $Ti_{0.17}Zr_{0.08}V_{0.35}Cr_{0.1}Ni_{0.3}$ alloy.

The exchange current density I_0 can be calculated by the following formula supposing that the surface status of the elec-

Table 3
The contact resistance R_{pp} between alloy particles, charge-transfer reaction resistance R_{ct}, polarization resistance R_p and exchange current density I_0 of the $La_{0.7}Mg_{0.3}Ni_{3.5}$ alloy and composite electrodes

Samples	Contact resistance between alloy particles, R_{pp} (mΩ)	Charge-transfer reaction resistance, R_{ct} (mΩ)	Polarization resistance, R_p (mΩ)	Exchange current density, I_0 (mA/g)
Alloy	747.1	327.8	211.5	79.6
Composite	334.2	160.2	129.5	201.6

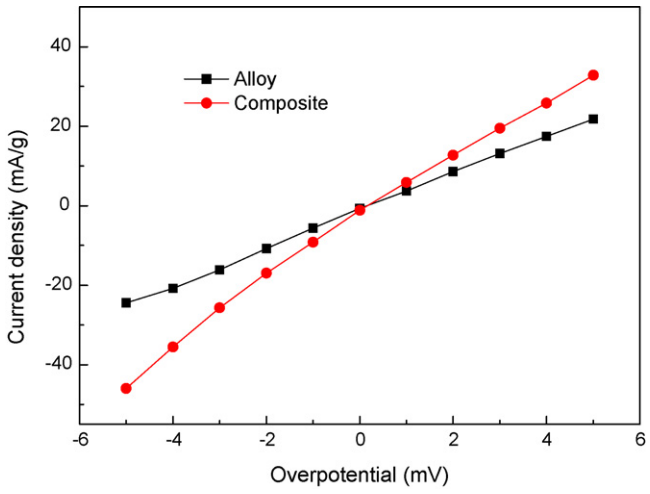

Fig. 8. Linear polarization curves of the $La_{0.7}Mg_{0.3}Ni_{3.5}$ alloy and composite electrodes at 50% DOD and 303 K.

trodes is similar [26]:

$$I_0 = \frac{RT}{FR_{ct}} \quad (2)$$

where R is the gas constant, T the absolute temperature, F the faraday constant, and R_{ct} is the charge-transfer resistance obtained from the EIS results. The I_0 values obtained from Eq. (2) are also tabulated in Table 3. It is found that the I_0 value of the composite electrode is 201.6 mA/g, which is much higher than that of the $La_{0.7}Mg_{0.3}Ni_{3.5}$ alloy electrode (79.6 mA/g). Moreover, the R_{ct} and I_0 of $Ti_{0.17}Zr_{0.08}V_{0.35}Cr_{0.1}Ni_{0.3}$ alloy electrode are 276.2 mΩ and 99.5 mA/g, respectively, which indicates that the improvements of electrode properties may be due to the intrinsic synergetic effect between two alloys in composite electrode.

Fig. 8 shows the linear polarization curves (LP) of the $La_{0.7}Mg_{0.3}Ni_{3.5}$ alloy and composite electrodes at 50% DOD and 303 K. There is a good linear dependence between the current and overpotential within a small overpotential range (±5 mV). The polarization resistances R_p, which can be determined from the slope of the related linear polarization curve, are listed in Table 3. It can be seen that the R_p of the composite electrode is 129.5 mΩ, which is lower than that of the $La_{0.7}Mg_{0.3}Ni_{3.5}$ alloy of 211.5 mΩ. This result is in good agreement with that of the EIS spectra.

All these results mentioned above indicate that the kinetics of the electrochemical hydrogen reaction in the composite electrode is significantly improved, which may be due to two aspects. One is the intrinsic synergetic effect between two alloys in composite electrode, which will account for the improvements of electrochemical kinetics. The other can be ascribed to the existence of C14 Laves phase in the composite alloy. According to the previous study [27], as an electrocatalyst in the Ti-based hydrogen storage alloy, C14 Laves phase could improve the charge-transfer reaction of metal hydride electrode in KOH electrolyte because it was a Ni-rich phase. Further investigations on the mechanism are being carried out in our laboratory.

4. Conclusions

Novel hydrogen storage composite is synthesized through ball milling the powders mixture of $La_{0.7}Mg_{0.3}Ni_{3.5}$ and $Ti_{0.17}Zr_{0.08}V_{0.35}Cr_{0.1}Ni_{0.3}$ alloys. It is found that the $La_{0.7}Mg_{0.3}Ni_{3.5}$ alloy and $Ti_{0.17}Zr_{0.08}V_{0.35}Cr_{0.1}Ni_{0.3}$ alloy maintain their respective phase structures in the composite. The average particle size of composite is less than 50 μm according to the SEM micrograph. However, the cyclic stability of the composite is greatly improved compared to that of the $La_{0.7}Mg_{0.3}Ni_{3.5}$ alloy. It is found that the cyclic retention rate C_{100}/C_{max} of composite electrode increases significantly to 62.3%, which is much higher than that (31.2%) of the $La_{0.7}Mg_{0.3}Ni_{3.5}$ alloy electrode. This improvement can be ascribed to the enhanced anti-corrosion behaviors of the composite in alkaline solution, in which the corrosion potential and current of the composite electrode are −0.702 V and 0.0862 A/g, respectively. Furthermore, the kinetics of the electrochemical hydrogen reaction is also improved for the composite electrode. According to the EIS and linear polarization measurement, the charge-transfer resistance R_{ct}, the polarization resistance R_p and the exchange current density I_0 of the composite electrode are 160.2 mΩ, 129.5 mΩ and 201.6 mA/g, respectively, which are superior to those of the $La_{0.7}Mg_{0.3}Ni_{3.5}$ alloy electrode (327.8 mΩ, 211.5 mΩ and 79.6 mA/g). These improvements can be attributed to the intrinsic synergetic effect between two alloys and the improved electrocatalytic activity of C14 Laves phase in the composite alloy.

Acknowledgements

This work was financially supported by the National Natural Science Foundation of China (nos. 50671098, 20473091 and 20573112) and the project sponsored by the Scientific Research Foundation for the Returned Overseas Chinese Scholars, State Education Ministry.

References

[1] T. Kohno, H. Yoshida, F. Kawashima, T. Inaba, I. Sakai, M. Yamamoto, M. Kanda, J. Alloys Compd. 311 (2000) L5.
[2] K. Kadir, T. Sakai, I. Uehare, J. Alloys Compd. 302 (2000) 112.
[3] F.L. Zhang, Y.C. Luo, A.Q. Deng, Z.H. Tang, L. Kang, J.H. Chen, Electrochim. Acta 52 (2006) 24.
[4] X.B. Zhang, D.Z. Sun, W.Y. Yin, Y.J. Chai, M.S. Zhao, Electrochim. Acta 50 (2005) 3407.
[5] J. Chen, N. Kuriyama, H.T. Takeshita, H. Tanaka, T. Sakai, M. Haruta, Electrochem. Solid-State Lett. 3 (6) (2000) 249.
[6] M. Li, S.M. Han, Y. Li, W. Guan, L.R. Mao, L. Hu, Electrochim. Acta 51 (2006) 5926.
[7] H.G. Pan, Y.F. Liu, M.X. Gao, Y.F. Zhu, Y.Q. Lei, Q.D. Wang, J. Alloys Compd. 351 (2003) 228.
[8] P. Zhang, Y.N. Liu, R. Tang, J.W. Zhu, X.D. Wei, S.S. Liu, G. Yu, Electrochim. Acta 51 (2006) 6400.
[9] Y.F. Liu, H.G. Pan, M.X. Gao, Y.F. Zhu, Y.Q. Lei, Q.D. Wang, Int. J. Hydrogen Energy 29 (2004) 297.
[10] T. Kohno, H. Yoshida, M. Kanda, J. Alloys Compd. 363 (2004) 254.
[11] B. Liao, Y.Q. Lei, L.X. Chen, G.L. Lu, H.G. Pan, Q.D. Wang, J. Alloys Compd. 376 (2004) 186.

[12] H.G. Pan, Q.W. Jin, M.X. Gao, Y.F. Liu, R. Li, Y.Q. Lei, J. Alloys Compd. 373 (2004) 237.
[13] X.B. Zhang, D.Z. Sun, W.Y. Yin, Y.J. Chai, M.S. Zhao, Electrochim. Acta 50 (2005) 1957.
[14] H.G. Pan, Y.J. Yue, M.X. Gao, X.F. Wu, N. Chen, Y.Q. Lei, Q.D. Wang, J. Alloys Compd. 397 (2005) 269.
[15] H.G. Pan, Y.F. Zhu, M.X. Gao, Y.F. Liu, R. Li, Y.Q. Lei, J. Alloys Compd. 370 (2004) 254.
[16] M. Tsukahara, K. Takahashi, T. Mishima, A. Isomura, T. Sakai, J. Alloys Compd. 253/254 (1997) 583.
[17] M. Tsukahara, K. Takahashi, T. Mishima, A. Isomura, T. Sakai, J. Alloys Compd. 236 (1996) 151.
[18] Y.J. Chai, Z.Y. Li, W.Y. Yin, X.B. Zhang, M.S. Zhao, J. Appl. Electrochem. 36 (7) (2006) 739.
[19] H.G. Pan, Y.F. Liu, M.X. Gao, Y.Q. Lei, Q.D. Wang, J. Electrochem. Soc. 150 (5) (2003) A565.
[20] Q.F. Tian, Y. Zhang, Z.C. Tan, L.X. Sun, F. Xu, H.T. Yuan, Acta Phys. Chim. Sin. 22 (3) (2006) 301.
[21] Q.F. Tian, Y. Zhang, Z.C. Tan, L.X. Sun, F. Xu, T. Zhang, H.T. Yuan, Trans. Nonferrous Met. Soc. China 16 (2006) 497.
[22] H.D. Jung, A. Alfantazi, Electrochim. Acta 51 (2006) 1806.
[23] C.N. Cao, The Principles of Corrosion Electrochemistry, 2nd ed., Chemical Industry Press, Beijing, 2004, 120–122.
[24] N. Kuriyama, T. Sakai, H. Miyamura, I. Uehara, H. Ishikawa, T. Iwasaki, J. Electrochem. Soc. 139 (1992) L72.
[25] Q.F. Tian, Y. Zhang, L.X. Sun, F. Xu, Z.C. Tan, H.T. Yuan, T. Zhang, J. Power Sources 158 (2006) 1463.
[26] N. Kuriyama, T. Sakai, H. Miyamura, I. Uehara, H. Ishikawa, J. Alloys Compd. 202 (1993) 183.
[27] H.H. Lee, K.Y. Lee, J.Y. Lee, J. Alloys Compd. 239 (1996) 63.